Photonic generation of amplitude- and phase-modulated microwave signals with frequency and modulation bit-rate tunability

Shuang Liu (刘 双)*, Zuping Qian (钱祖平), Rong Wang (王 荣), Tao Pu (蒲 涛), and Tao Fang (方 涛)

Institute of Communications Engineering, PLA University of Science and Technology, Nanjing 210007, China

**Corresponding author: youyou1985@xnmsn.cn*

Received May 28, 2012; accepted August 7, 2012; posted online November 30, 2012

A photonic approach for the generation of an amplitude- and phase-modulated microwave signal with tunable frequency and modulation bit-rate is proposed and demonstrated. Two coherent optical wavelengths are generated based on external modulation by biasing a Mach–Zehnder modulator (MZM) at the minimum transmission point to generate ±1-order optical sidebands while suppressing the optical carrier. The two sidebands are sent to a circulator and are then spectrally separated by a fiber Bragg grating notch filter. With one sideband being amplitude-modulated at another MZM and the other being phase-modulated at a phase modulator, a frequency-tunable amplitude- and phase-modulated microwave signal is generated by beating the two sidebands at a photodetector. The proposed technique is investigated theoretically and experimentally. As a result, a 20-GHz amplitude-modulated, 20-GHz phase-modulated, and 25-GHz amplitude- and phase-modulated microwave signals with tunable modulation bit-rate are experimentally generated.

OCIS codes: 040.2840, 350.4010, 060.3735.

doi: 10.3788/COL201210.120401.

The photonic generation of microwave and millimeter-wave (MMW) signals is considered a promising technique for providing high-frequency, low-phase-noise microwave and MMW signals that can meet the demands of numerous applications such as broadband radio access networks, radar systems, antenna remoting, and phased array antennas[1−4].

In communication systems, the electrical generation of radio signals at MMW frequencies is expensive and energy inefficient, and the distribution of such signals via wireless or coaxial methods is highly challenging when compared with optical methods[5]. Moreover, the electrical modulation of a baseband data to a high-frequency microwave requires a high-frequency modulator that is difficult to manufacture. However, photonic generation and the processing of microwave and MMW signals have attracted considerable interest because this approach not only overcomes the inherent bottleneck of traditional electronic approaches but also offers attractive features such as large time-bandwidth products and immunity to electromagnetic interference[6−8].

Different approaches have been proposed for the generation of microwave and MMW signals based on optical heterodyne techniques[9−12]. Among these microwave photonic methods, the techniques that use external-modulation have shown great potential. A stable, highly pure, and high-frequency microwave signal can be obtained because the optical sidebands are perfectly coherent, and the frequency of the generated signals can also be tuned by using the low-frequency microwave driving signal of the modulator[13−15].

Various techniques for the generation of phase-coded microwave pulses were demonstrated[16−22]. A phase-coded microwave pulse was generated based on optical pulse shaping by using a spatial light modulator[16,17] and a photonic microwave delay-line filter[18] in which the phase shift of a specific bit was achieved by an additional time-delay to the specific tap. A phase-coded microwave pulse could also be generated by incorporating an optical phase modulator (PM) in one arm of a Mach–Zehnder interferometer[19] or in a Sagnac interferometer[20]. A differential group delay module[21] and a polarization-maintaining fiber Bragg grating (FBG)[22] were utilized to make two sidebands orthogonally polarized, respectively. In addition, a polarization modulator was used to replace the PM. However, these techniques above only considered the microwave signal phase. Advanced data modulation format is playing an ever-increasing role within the optical communications community. For example, phase modulation provides better receiver sensitivity and tolerance to nonlinear effects, and quadrature amplitude modulation provides increased spectral efficiency and tolerance to chromatic dispersion.

In this letter, we propose and demonstrate a novel approach for generating an amplitude and phase-modulated microwave signal with tunable frequency and modulation bit-rate, which can be widely-used in digital cable TV transmission and multichannel multipoint distribution services system, with its flexible configuration and excellent performance. To emphasize, the proposed technique can also easily achieve amplitude-modulation or phase-modulation for a high-frequency microwave signal. The principle is discussed in detail in this work. Mathematical models are developed to consider perturbations on the generated microwave modulated-signal caused by the phase fluctuations of the microwave driving signal, which is applied to the external modulator and to the optical carrier that feeds the external modulator. Closed-form expression of the generated microwave modulated-signal is derived. The calculated expression of the generated amplitude- and phase-modulated microwave signal indicates that

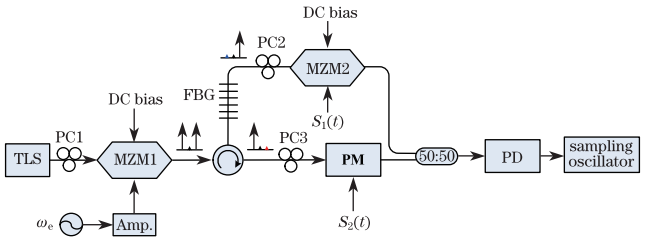

Fig. 1. Schematic of the proposed system for photonic generation of MMW signals.

its phase noise is determined only by the phase noise of the microwave driving signal. Thus, a 20-GHz amplitude-modulated, 20-GHz phase-modulated, and 25-GHz amplitude- and phase-modulated microwave signals with tunable modulation bit-rate are experimentally generated.

Figure 1 shows the schematic of the proposed system for photonic generation of MMW signals. A continuous light wave from a tunable laser source (TLS Agilaet 81989A) is sent to the first MZM (MZM1) through a polarization controller (PC1), which is used to ensure that the incident light is well-aligned with the principal axis of the MZM1. A sinusoidal microwave driving signal with an appropriate power level is applied through an amplifier to the MZM1 that is biased at the minimum transmission point (MITP) by tuning the DC bias, which can generate ±1-order optical sidebands while suppressing the optical carrier. The two optical sidebands are sent to a circulator and separated by a FBG notch filter. One sideband is sent to the second MZM (MZM2) through a PC (PC2), and the other is sent to the PM through a PC (PC3). The modulation signals $S_1(t)$ and $S_2(t)$ with amplitudes of V_1 and V_2 are applied to the MZM2 and PM, respectively. The amplitude- and the phase-modulated optical sidebands are then coupled by a 3-dB optical coupler (OC). By beating the two sidebands at a photodector (PD), an amplitude and phase-modulated microwave signal with a frequency that is two times the frequency of the microwave driving signal is generated.

Mathematically, the optical signal at the output of the MZM1 can be expressed as[23]

$$E(t) = E_{\rm o}J_1(\beta)\exp\{{\rm j}[(\omega_{\rm o}+\omega_{\rm e})t+\phi_{\rm o}(t)+\phi_{\rm e}(t)]\} + E_{\rm o}J_1(\beta)\exp\{{\rm j}[(\omega_{\rm o}-\omega_{\rm e})t+\phi_{\rm o}(t)-\phi_{\rm e}(t)]\}, \quad (1)$$

where $\omega_{\rm o}$ and $\omega_{\rm e}$ are the angular frequencies of the optical carrier and of the microwave driving signal applied to the MZM1, respectively; $E_{\rm o}J_{\rm l}(\beta)$ is the amplitude of ±1-order optical sidebands, and $E_{\rm o}$ is the electric field amplitude of the optical carrier, $J_{\rm n}$ is the Bessel function of the first kind of order n. $\phi_{\rm o}$(t) and $\phi_{\rm e}$(t) are two independent random processes that introduce phase fluctuations to the optical carrier and to the microwave driving signal, respectively.

The optical signal at the output of the OC is

$$E(t) = \sqrt{2}/2E_{\rm o}J_1(\beta) \cdot (V_1/V_{\pi 1})\cdot s_1(t)\exp\{{\rm j}[(\omega_{\rm o}+\omega_{\rm e})t+\phi_{\rm o}(t)+\phi_{\rm e}(t)]\} + \sqrt{2}/2E_{\rm o}J_1(\beta)\exp\{{\rm j}[(\omega_{\rm o}-\omega_{\rm e})t + \phi_{\rm o}(t)-\phi_{\rm e}(t)+\pi(V_2/V_{\pi 2})\cdot s_2(t)]\}, \quad (2)$$

where $V_{\pi 1}$ and $V_{\pi 2}$ are the half-wave voltages of the MZM2 and the PM. Finally, the amplitude and phase-modulated microwave signal at the output of the PD is

$$i(t) = A\cdot(V_1/V_{\pi 1}) \cdot s_1(t)\exp\{{\rm j}[2\omega_{\rm e}t+2\phi_{\rm e}(t)-\pi(V_2/V_{\pi 2})\cdot s_2(t)]\}, \quad (3)$$

where the coefficient A includes the effect of $E_{\rm o}J_1(\beta)$ and the responsivity of the PD. As shown by Eq. (3), a frequency-doubled amplitude and phase-modulated microwave signal is generated. Equation (3) also shows that the phase fluctuation of the modulated microwave signal is not affected by the phase fluctuation $\phi_{\rm o}$(t) of the optical carrier. However, the phase fluctuation $\phi_{\rm e}$(t) of the microwave driving signal will contribute to the phase noise of the generated electrical signal. Thus, a better modulated microwave signal is obtained when a purer microwave driving signal is applied.

In the proposed system, the subsystem before the circulator is designed to provide two coherent optical wavelengths. The two times frequency scheme, which is simple and common, is used in our experiment. The principle remains the same for the four, six, eight, and twelve times frequency scheme, which enables the proposed system to take advantage of photonic technologies. However, as the frequency becomes higher, the demands on the device will increase, such as the demand on PD.

An experiment based on the setup shown in Fig. 1 is performed. A FBG notch filter is fabricated in a hydrogen-loaded fiber by using a frequency-doubled argon-ion laser operating at 244 nm and a 10-cm-long uniform phase mask. The transmission spectrum of the FBG, as shown in Fig. 2, has a bandwidth of approximately 0.05 nm. Therefore, if the wavelength of the optical carrier is fixed, the frequency of the microwave driving signal is only allowed to be tuned in a 6.25-GHz range at most. However, the TLS is used to ensure large

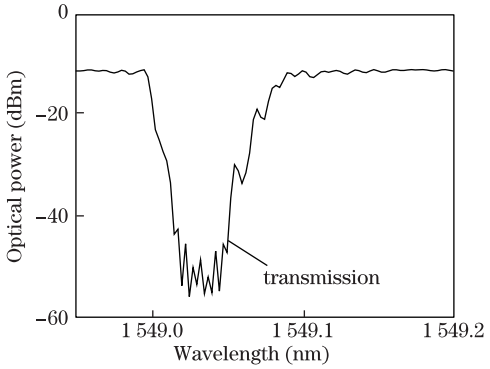

Fig. 2. Transmission spectrum of the FBG.

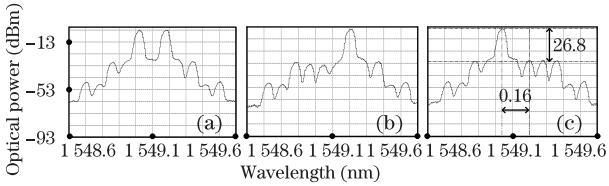

Fig. 3. Optical spectra of the ±1-order sidebands: (a) two sidebands at the output of the MZM1; (b) transmitted +1-order sideband; (c) reflected –1-order sideband.

frequency tunability in our proposed experiment system, because the wavelength of –1-order optical sideband can be always placed at the stopband of the FBG notch filter by tuning the wavelength of the optical carrier.

When the wavelength of the optical carrier is 1 549.102 nm and the frequency of the microwave driving signal from a signal generator (Anritsu MP1763C) is 10 GHz, the optical spectra of the ±1-order optical sidebands that are measured by an optical spectrum analyzer (Anritsu MS9710C) are as shown in Fig. 3. The generated ±1-order sidebands with the optical carrier suppressed in Fig. 3(a) is detected at the output port of the MZM1. The transmitted +1-order sideband in Fig. 3(b) is detected at the input port of the PC2. The reflected –1-order sideband in Fig. 3(c) is detected at the input port of the PC3. The power of the optical carrier is 25 dB lower than those of the two sidebands, and the isolation between the two optical sidebands is approximately 26.8 dB, which adequately satisfies the experiment demand.

To demonstrate that the proposed technique can generate amplitude-modulated, phase-modulated, amplitude and phase-modulated microwave signals, we complete next three experiments, respectively.

In the photonic generation of amplitude-modulated microwave signal experiment, a 10-Gb/s digital signal, which is a pseudorandom bit sequence from a bit error rate tester, is amplified and then applied to the MZM2 to achieve amplitude modulation. Figure 4(a) shows the binary amplitude modulation signal with a length of 8 bits. Given that the +1-order sideband is amplitude-modulated, whereas the –1-order sideband is not modulated, the amplitude-modulated microwave signal is generated at the output of the PD, as monitored by a sampling oscilloscope (LeCroy NRO9000).

The generated 20-GHz amplitude-modulated microwave signal with 0.8-ns time duration corresponding to the modulation signal in Fig. 4(a) is shown in Fig. 4(b). In the experiment, the power of the modulation signal after amplification is approximately 30 dBm, which is attenuated to be 24 dBm (P=251.19 mW) because of the max RF input power of the MZM2 (JDS Uniphase OC-192). Thus, the amplitude V_1 of the modulation signal is calculated to be approximately 3.54 V, based on $V = \sqrt{P \cdot R}$ for a square wave, where the input impedance of the MZM2, R, is 50 Ω[21]. Because the half-wave voltage of the MZM2 is approximately 6.8 V, the amplitudes corresponding to "1" and "–1" are calculated to be 0.94 and –0.94 according to Eq. (3), with the effect of the coefficient A. Figure 4(c) shows the amplitude information of the amplitude-modulated signal recovered using the coherent detection method. The amplitudes corresponding to "1" and "–1" are 0.6 and –0.87.

In the photonic generation of phase-modulated microwave signal experiment, the change is that the +1-order sideband is not modulated, while the –1-order sideband is phase-modulated, compared with the first experiment. The generated 20-GHz phase-modulated microwave signal with 0.8-ns duration corresponding to the modulation signal in Fig. 5(a) is shown in Fig. 5(b). The power of the modulation signal applied to the PM (EOSPACE AZ-AV5-40-PFU-SFU) is approximately 15 dBm (31.25 mW). Thus, the amplitude V_2 of the modulation signal is calculated to be approximately 1.25 V for a square wave. As the half-wave voltage of the PM is approximately 4.0 V, the phase shifts corresponding to "1" and "–1" are calculated to be 56.25° and –56.25°, according to Eq. (3). Therefore, the phase shift difference between "1" and "–1" is around 112.5°. Figure(c) shows the phase information of the phase-modulated signal recovered using the coherent detection method. The maximum phase shift difference between "1" and "–1" is 116.5°, which agrees well with the theoretical value.

In the photonic generation of amplitude and phase-modulated microwave signal experiment, the change is that the +1-order sideband is amplitude-modulated while the –1-order sideband is phase-modulated, compared with the two previously discussed experiments. To demonstrate the frequency and the modulation data-rate tunability, the frequency of the microwave driving signal is tuned to 12.5 GHz, and the modulation data-rate is tuned to 2.5 Gb/s. The generated 25-GHz amplitude and phase-modulated microwave sig-

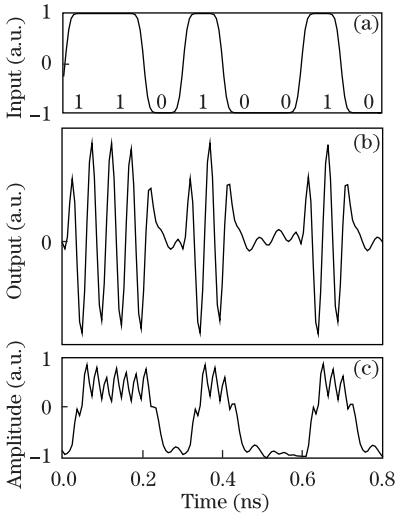

Fig. 4. (a) Amplitude-modulated signal $S_1(t)$; (b) generated 20 GHz amplitude-modulated microwave signal; (c) recovered amplitude information from the signal in (b).

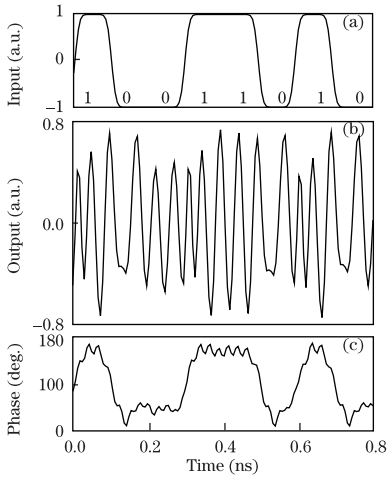

Fig. 5. (a) Phase-modulated signal $S_2(t)$; (b) generated 20 GHz phase-modulated microwave signal; (c) recovered phase information from the signal in (b).

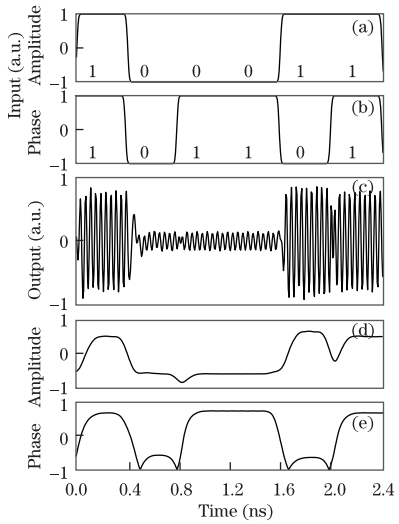

Fig. 6. (a) Amplitude-modulated signal $S_1(t)$; (b) phase-modulated signal $S_2(t)$; (c) generated 25-GHz amplitude- and phase-modulated microwave signal; (d) recovered amplitude information from the signal in (c); (e) recovered phase information from the signal in (c).

nal with 2.4-ns time duration corresponding to the amplitude modulation signal in Fig. 6(a) and the phase modulation signal in Fig. 6(b) is shown in Fig. 6(c). The generated waveform obviously has two amplitudes corresponding to the amplitude modulation signal, and there will be an abrupt phase change in the waveform when the phase modulation data changes. Figures 6(d) and (e) shows the amplitude and phase information recovered using the coherent detection method corresponding to the modulation signals in Figs. 6(a) and (b).

To complete the demodulation process, the coherent detection method is used. In the experiment in which the signal is both amplitude- and phase-modulated, the modulated microwave signal generated by the proposed system is divided into two branches for the extraction of the components in phase and in quadrature, respectively, by multiplying by a cosine (or a sine) with the same frequency and by a low-pass filter. Subsequently, the computer can obtain the demodulated signals through corresponding program calculations and decisions.

In conclusion, we propose and demonstrate a novel approach for the generation of an amplitude- and phase-modulated microwave signal with tunable frequency and modulation bit-rate. The beating of the optical amplitude-modulated sideband and the optical phase-modulated sideband can generate an amplitude- and phase-modulated microwave signal with tunable frequency and modulation bit-rate. The calculated expression of the generated amplitude- and phase-modulated microwave signal indicates that the phase noise is determined only by the phase noise of the microwave driving signal. Thus, 20-GHz amplitude-modulated, 20-GHz phase-modulated, and 25-GHz amplitude- and phase-modulated microwave signals with tunable modulation bit-rate are experimentally generated. The modulation information of modulated signals that are recovered by using the coherent detection method is also experimentally demonstrated, which agrees well with the theoretical value.

This work was supported by the National Natural Science Foundation of China (Nos. 61032005 and 61177065) and the National "973" Project of China (No. 2012CB315603). The authors would like to thank Professor Pan of the Microwave Photonic Research Laboratory in Nanjing University of Aeronautics and Astronautics for his productive discussions on this work.

References

1. A. J. Seeds, IEEE Trans. Microw. Theor. Technol. **50,** 877 (2002).
2. S. J. B. Yoo, R. P. Scott, D. J. Geisler, N. K. Fontaine, and F. M. Soares, IEEE Trans. Terahertz Sci. Technol. **2,** 167 (2012).
3. J. J. O'Reilly, P. M. Lane, R. Heidemann, and R. Hofstetter, Electron. Lett. **28,** 2309 (1992).
4. T. X. H. Huang, X. Yi, and R. A. Minasian, Opt. Express **19,** 6231 (2011).
5. P. Shen, N. J. Gomes, P. A. Davies, W. P. Shillue, P. G. Huggard, and B. N. Ellison, in *Proceedings of Microwave Photonics 2003* 189 (2003).
6. G. Qi, J. Yao, J. Seregelyi, S. Paquet, and C. Bélisle, Proc. SPIE **5579,** 673 (2004).
7. G. Qi, J. Yao, J. Seregelyi, S. Paquet, and C. Bélisle, J. Lightwave Technol. **23,** 2687 (2005).
8. H.-J. Song, N. Shimizu, T. Furuta, K. Suizu, H. Ito, and T. Nagatsuma, J. Lightwave Technol. **26,** 2521 (2008).
9. X. Chen, Z. Deng, and J. Yao, IEEE Trans. Microw. Theor. Technol. **54,** 804 (2006).
10. J. Zhang, H. Chen, M. Chen, T. Wang, and S. Xie, Opt. Lett. **32,** 1020 (2007).
11. C.-T. Lin, P.-T. Shih, J. Chen, W.-Q. Xue, P.-C. Peng, and S. Chi, IEEE Photon. Technol. Lett. **20,** 1027 (2008).
12. S. Pan and J. Yao, Opt. Express **17,** 5414 (2009).
13. J. Zhang, H. Chen, M. Chen, T. Wang, and S. Xie, IEEE Photon. Technol. Lett. **19,** 1057 (2007).
14. S. Pan, C. Wang, and J. Yao, in *Proceedings of OFC 2009* JWA51 (2009).
15. S. Pan and J. Yao, IEEE Trans. Microw. Theor. Technol. **58,** 1967(2010).
16. J. D. McKinney, D. E. Leaird, and A. M. Weiner, Opt. Lett. **27,** 1345 (2002).
17. J. Chou, Y. Han, and B. Jalali, IEEE Photon. Technol. Lett. **15,** 581 (2003).
18. Y. Dai and J. Yao, Opt. Lett. **32,** 3486 (2007).
19. H. Chi and J. Yao, IEEE Photon. Technol. Lett. **19,** 768 (2007).
20. Z. Li, W. Li, H. Chi, X. Zhang, and J. Yao, IEEE Photon. Technol. Lett. **23,** 712 (2011).
21. H. Chi and J. Yao, IEEE Microw. Wireless Compon. Lett. **18,** 371 (2008).
22. Z. Li, M. Li, H. Chi, X. Zhang, and J. Yao, IEEE Microw. Wireless Compon. Lett. **21,** 694 (2011).
23. G. Qi, J. Yao, J. Seregelyi, S. Paquet, C. Bélisle, X. Zhang, K. Wu, and R. Kashyap, J. Lightwave Technol. **24,** 4861 (2006).